Late Holocene *Ameghinomya antiqua* shells from the Beagle Channel: A multi-proxy approach to palaeoenvironmental and palaeoclimatic reconstruction

Gisela A. Morán [a,b,i,*], Sol Bayer [a,b], Lars Beierlein [f], Juan J. Martínez [d], Santiago Benitez-Vieyra [a,e], Andreas Mackensen [f], Thomas Brey [f,g,h], Sandra Gordillo [a,c]

[a] *Universidad Nacional de Córdoba, Facultad de Ciencias Exactas, Físicas y Naturales, Córdoba, Argentina*
[b] *Consejo Nacional de Investigaciones Científicas y Tecnológicas (CONICET), Centro de investigaciones en Ciencias de la Tierra, (CICTERRA), Avda. Vélez Sarsfield 1611, X5016GCA, Córdoba, Argentina*
[c] *Consejo Nacional de Investigaciones Científicas y Tecnológicas (CONICET), Instituto de Antropología de Córdoba (IDACOR), Av. Hipólito Yrigoyen 174, X5016GCA, Córdoba, Argentina*
[d] *Consejo Nacional de Investigaciones Científicas y Tecnológicas (CONICET), Instituto de Ecorregiones Andinas (INECOA-UNJu), Lab. Ecología Evolutiva y Biogeografía, C. Gorriti 237, San Salvador de Jujuy, Jujuy, Argentina*
[e] *Consejo Nacional de Investigaciones Científicas y Tecnológicas (CONICET), Instituto Multidisciplinario de Biología Vegetal (IMBIV), Avda. Vélez Sarsfield 1611, X5016GCA, Córdoba, Argentina.*
[f] *Alfred-Wegener-Institute, Helmholtz Centre for Polar and Marine Research (AWI), Am Handelshafen 12, 27570, Bremerhaven, Germany.*
[g] *Helmholtz Institute for Functional Marine Biodiversity at the University of Oldenburg (HIFMB), Ammerländer Heerstraße 231, 23129 Oldenburg, Germany*
[h] *University of Bremen, Bibliothekstraße 1, 28359 Bremen, Germany*
[i] *Consejo Nacional de Investigaciones Científicas y Tecnológicas (CONICET), Instituto de Diversidad y Ecología Animal (IDEA), Avda. Vélez Sarsfield 299, X5016GCA, Córdoba, Argentina*

ARTICLE INFO

ABSTRACT

It is important to understand the historical precedents of current situations to be able to anticipate where the current global environmental and climatic change may lead. Geo-historical data provide information beyond the limitations of instrumental data. This study aims to reconstruct components of the palaeoclimatic and palaeoenvironmental history of the Beagle Channel (BC) during the Late Holocene by using *Ameghinomya antiqua* shells. We use fossil and modern shells in a comparative analysis through a multiproxy approach, i.e., shell morphometrics, shell growth, and stable oxygen isotope ratios. A holistic analysis of all the proxies indicates that higher productivity occurred around 3542 yr B.P. in the BC, evidenced by more significant growth, size, and longevity in fossil specimens. In addition, smaller ligaments, cardinal teeth, and the pallial sinus in fossil specimens indicate a low-energy environment typical of a marine archipelago. Lastly, palaeotemperatures are estimated to be warmer than today, although the intensity may be overestimated due to the freshwater inflow that would change the salinity of the BC waters. Further analysis in Late-Holocene shells is essential for a more detailed environmental reconstruction around the southern tip of South America.

1. Introduction

In recent decades, climate changes have altered the structure and functioning of marine ecosystems (IPCC, 2014; Poloczanska et al., 2016; Hillebrand et al., 2018). The projections indicate that the global mean ocean temperature will continue to warm by between 0.6 and 2 °C during the current century (IPCC, 2014), illustrating the urgent need to understand the impacts on marine biota. Understanding the past climate is crucial for anticipating future climate change and its impacts on marine ecosystems. The interaction between environmental shifts and

marine biota has been studied, mainly using observational and experimental data (Harley et al., 2006). However, environmental proxy data with high temporal resolution from pre-instrumental times are valuable for (i) understanding past environmental and climatic trends and (ii) establishing ecological baselines and reference conditions (Dietl et al., 2015; Dietl et al., 2019; Lockwood and Mann, 2019).

Although climate change occurs on a global scale, ecological impacts are local and vary between different regions (Turner and Marshall, 2011; Constable et al., 2014; Franco et al., 2020). High-latitude ecosystems, such as the sub-Antarctic Beagle Channel (BC) region, appear to be particularly sensitive to climate change (IPCC, 2014). Its recent geological history includes notable changes in water masses and their circulation that have greatly influenced the distribution and configuration of benthic marine communities (Gordillo and Isla, 2011; Gordillo et al., 2013). Previous studies reported changing climatic and environmental conditions for the southern tip of South America throughout the Late Holocene (Lamy et al., 2002). In particular, the BC was affected by transgression/regression events during the Holocene, which, together with complex geomorphological changes, caused the western area of the Argentine BC to become a marine archipelago from 7500 to 4000 yr B.P. (Rabassa et al., 1986; Gordillo et al., 1993; Gordillo et al., 2005; Rabassa et al., 2009). Warming has also been identified between 4500 and 3000 yr B.P. (Panarello, 1987; Obelic et al., 1998; Candel et al., 2009; Gordillo et al., 2014, 2015), although there are still some uncertainties about its origin and magnitude (see Pendall et al., 2001; Nielsen et al., 2004; Renssen et al., 2005; Lamy et al., 2010; Etourneau et al., 2013).

In marine environments, high-resolution proxy data derived from biogenic carbonate is one of the most important and commonly used sources of information about the climate of the last several thousand years (Wanamaker et al., 2011; Schöne and Gillikin, 2013; Butler and Schöne, 2017; Gillikin et al., 2019; Peharda et al., 2021). In the high latitudes, bivalve shells are the only widespread biogenic archive recording information on climate and the marine environment at a multi-decadal and sub-annual temporal resolution (Schöne and Gillikin, 2013). However, in Southern South America, the sclerochronological archive of environmental, climatic and growth information recorded in bivalve shells remains largely unexplored. The striped clam, *Ameghinomya antiqua* (King, 1832), is an important high latitude bio-archive and can be found both on the present beaches of the Southern tip of South America and in its Holocene and Pleistocene marine coastal deposits (Feruglio, 1950; Reid and Osorio, 2000; Boretto et al., 2013, 2014, 2019). Previous studies at different locations in Argentinian Patagonia indicate that the anatomical features of *A. antiqua* shells may constitute suitable environmental proxies (Boretto et al., 2014; Morán et al., 2018). In addition, the accretion growth and geochemical properties of this species provides valuable high-resolution data of pre-instrumental times (Rubo et al., 2018; Boretto et al., 2019).

In the BC, several palaeoecological records have provided valuable palaeoclimatic proxies that have contributed to the reconstruction of Holocene climate and environmental change (Candel et al., 2009, 2013, 2018; Gordillo et al., 2005; Gordillo, 2009; among others). However, the interpretation of stable isotope-derived palaeoclimatic information is often complex given the estuarine dynamics of the BC (Obelic et al., 1998; Isla et al., 1999; Gordillo et al., 2011, 2014, 2015), and there is a need to improve, deepen and broaden the range of tools, to help to unravel the environmental history of the area. This work aims to reconstruct components of the palaeoclimate and palaeoenvironmental history of the BC during the Late Holocene, using *A. antiqua* shells. Through a multi-proxy approach, it is possible to achieve a more comprehensive and accurate environmental interpretation. For this, we used the shape, size, growth, and stable oxygen isotopes ($\delta^{18}O_{shell}$) of *A. antiqua* shells. This study is a step towards providing new evidence for high latitude palaeoclimate and palaeoenvironment reconstruction in an area where long-term time-series and observational data for the present and the past are scarce.

2. Background

2.1. Regional setting

The BC (Fig. 1) is located within the southernmost tip of South America, between Isla Grande de Tierra del Fuego to the north and Isla Navarino to the south, joining the Atlantic and Pacific oceans. The channel comprises an area of 300 km², with an average width of 5 km and a maximum depth of 300 m. Situated close to the Antarctic Circumpolar Current, the region experiences a temperate-cold maritime climate, with winds predominantly coming from the west-southwest or the south. Monthly mean sea surface temperatures (SST) in the region range from 4 to 10 °C (Gordillo et al., 2015). Sea surface salinity varies between 27 and 31.5 PSU with minimum values during summer (Almandoz et al., 2011; Aguirre et al., 2012), which vary considerably along the channel. Annual precipitation ranges between 500 and 600 mm (Bujalesky et al., 2008). The channel shows typical characteristics of a fjord, with estuarine dynamics controlled by extensive fluvial inputs and by tidal currents from both the east and the west (Isla et al., 1999).

2.2. Geological background

The current geomorphology of the BC is a tectonic valley, which has been shaped by the effects of successive glaciations and marine events (Rabassa et al., 2000; Bujalesky, 2007; Bujalesky et al., 2021) that occurred during the Quaternary period. At about 9400 yr B.P., the area was a glacial lake with a water level up to 30 m above the present sea level. In the early Holocene (before 8200 yr B.P.), the BC was transformed into a marine channel by the entry of water from the surrounding oceans (Rabassa et al., 1986, 2000; Gordillo et al., 1993). This marine transgression left Holocene marine deposits, mainly in the form of raised beaches, distributed along both coasts (north and south) of the BC (Gordillo et al., 1992; Gordillo, 1999). These deposits contain rich marine fauna (especially mollusc shells), the taphonomy and palaeoecology of which were previously studied (Gordillo et al., 2005; Gordillo, 2009; among other works). During mid-Holocene times (ca 7500–4000 yr B.P.), the western area of the Argentine BC became a marine archipelago. Today it is a freshwater environment formed by a series of low, rounded bedrock hills, an ice-scoured terrain, surrounded by interconnected depressions filled with freshwater lakes and ponds and peat bogs. The fossil marine deposits are scattered along Lapataia Bay, Lago Roca, including the Cormoranes Archipelago and the Ovando and Lapataia rivers (Fig. 1D). Both rivers contain elevated beaches with mollusc assemblages, which have been studied in previous works (Gordillo et al., 1993; Gordillo et al., 2005).

2.3. Autoecology of Ameghinomya antiqua

The striped clam *A. antiqua* (Bivalvia; Veneriade) is a benthic species typical of the Magellanic region (Balech and Ehrlich, 2008). It is distributed along the Atlantic Ocean coasts from 34°S (Uruguay) to 54°S (Beagle Channel) and along the Pacific coasts, extending to Callao (13°S) in Perú (Castellanos, 1967). The species inhabits shallow sandy-soft bottom substrates, from the intertidal to around 50 m water depth, preferably in temperate-cold waters (Rosenberg, 2009). Sexes are separate, and reproduction is external (Stead et al., 1997). It is considered a strict suspension feeder, not extending its short and fused siphons above the sediment surface (Lardies et al., 2001). In Patagonia Argentina, *A. antiqua* has a lifespan of up to 16 years (Escati-Peñaloza et al., 2010; Boretto et al., 2019). However, some longer-lived specimens (34 years old) have recently been reported in the San Jorge Gulf (Rubo et al., 2018).
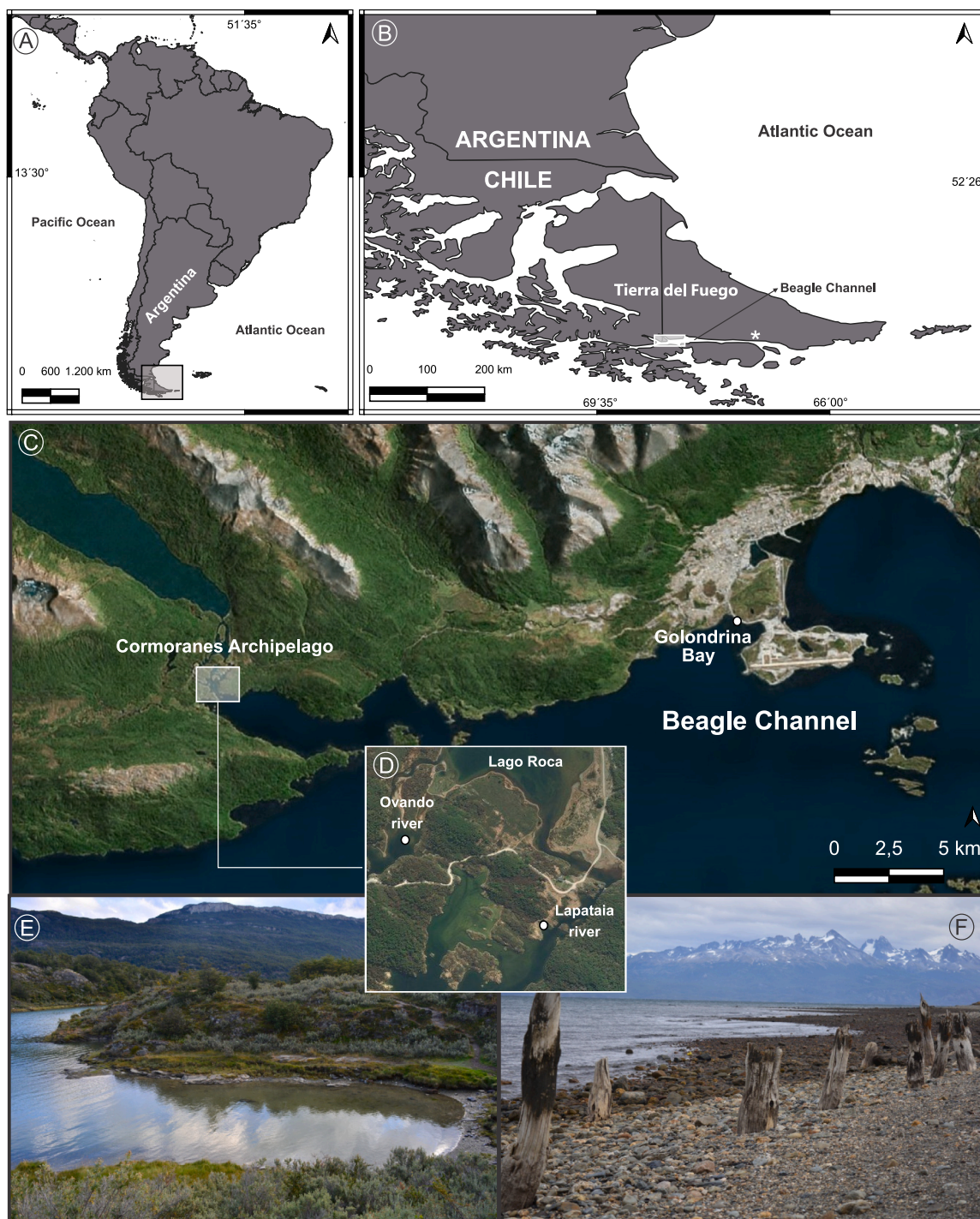
Fig. 1. Map of the study area in the southern tip of South America (A-B) and the different sampling sites (white dots) (C-F). Fossil shells of *A. antiqua* were recovered from Holocene raised marine deposits (C-D) located in the Lapataia (E) and Ovando rivers, in the Cormoranes Archipelago. Modern shells were sampled in Golondrina Bay (C and F). White star symbol gives the location of Lanaushuaia, where $\delta^{18}O_{water}$ samples were measured by Colonese et al. (2012) and Nicastro et al. (2020).

3. Materials and methods

3.1. Shell collection in the field

Modern adult shell specimens of *A. antiqua* were randomly hand-collected in February (summer) 2016 during the lowest tide of the month, at the undertow line off the coast in Golondrina Bay, located on the western side of the Ushuaia Peninsula, Ushuaia city (54° 49′50"S, 68° 19′49" W) (Fig. 1). The 43 shells had their ligaments and soft tissues still preserved.

The 36 fossil specimens were collected at the Cormoranes Archipelago in the Tierra del Fuego National Park. The shells were randomly hand-picked from raised beaches on the shores of the Ovando and Lapataia rivers (Entre Ríos island) (54°50′45"S, 68°33′55"W) (Fig. 1C-E). It is assumed that these assemblages are contemporary, according to malacological and taphonomic studies of these deposits (Gordillo et al., 1993; Gordillo, 1999). These specimens are currently stored in the palaeontological repository of the Centro de Investigaciones en Ciencias

de la Tierra (CICTERRA), Universidad Nacional de Córdoba (Argentina). For all analyses, we used the right valves only (both modern and fossils). For the morphometric analysis, it was essential to select shells with unbroken contours and visible internal structures.

3.2. Shell dating

After removing the periostracum and any adhering sediment from the outer surface, a fragment of one fossil shell was radiocarbon dated by Accelerator Mass Spectrometry (AMS) ^{14}C at the Poznań Radiocarbon Laboratory (Poland). Conventional radiocarbon ages were converted to calibrated ^{14}C ages (cal. yr B.P.) by the program Calib 7.0.4 (http://calib.qub.ac.uk/calib, Stuiver and Reimer, 1993) using the MARINE13 calibration data set (Reimer et al., 2013) and average ΔR offsets and errors based on the nearest published values (http://calib.or g/marine/).

3.3. Morphometric analysis

The right valves of modern ($N = 32$) and fossil ($N = 29$) shells of *A. antiqua* were used for linear and geometric morphometric approaches. Shell isometric size was analysed employing linear morphometrics. We applied geometric morphometrics to check for differences in shell shape regardless of size (see following paragraphs).

3.3.1. Linear morphometrics

Four shell variables were analysed: length (maximum anterior to posterior distance), height (maximum dorsal to ventral distance), width (maximum width of the umbo), and weight. The measurements were taken using a digital calliper (precision 0.01 mm) and a precision balance (0.1 g).

3.3.2. Geometric morphometrics

For geometric morphometric analysis, the interior of each right valve was photographed (Nikon Coolpix P-100 digital camera) (Fig. 2). On each image, twelve Type-I landmark points located on internal features

Fig. 2. Right valve of an *A. antiqua* specimen (ID #A8_542) with the location of Type I and III landmarks (white dots, numbered from 1 to 15) used to define the shape of the right shell and semi-landmarks along the outline (dashed line). The landmarks were: (1) umbo, (2) the ventral tip of the posterior cardinal tooth, (3) the middle cardinal tooth, (4) the ventral tip of the anterior cardinal tooth, (5) the scar of the lunule, (6, 7) the tips of the anterior adductor muscle scar, (8) the lower tip of the pallial sinus, (9) the tip of the pallial sinus, (10,11) the tips of the posterior adductor muscle scar, (12) the tip of the posterior hinge ligament, (13) posterior end, (14) ventral end, (15) anterior end.

of the shells, three Type-III landmarks on the ends of shells and 41 semilandmarks on the shell outline were marked with tpsDig2 (Rohlf, 2005) to quantify shape, following Morán et al. (2018). Landmark and semilandmark positions were rotated, scaled and translated through Generalised Procrustes Analysis using TpsRewl (Rohlf, 1999), minimising the bending energy matrix (for more details on geometric morphometric methodologies using landmarks cf. Bookstein, 1997; Adams et al., 2004; Zelditch et al., 2004). Centroid size, used as a non-dimensional proxy of shell size, was calculated to evaluate size differences independent of shape. We performed an ANCOVA (analysis of covariance) test using assemblage, centroid size (covariate) and the interaction term to assess statistical shape differences. The statistical significance of the interaction term could suggest unique allometric effects for each period. To assess allometric effects, we computed the multivariate regression between size and shape. Pairwise comparison of slope vectors was also performed. These analyses were implemented in the *geomorph* package (Adams et al., 2020) for R software (R Development Core Team, 2016, version 2.6.0). All ANOVA procedures were evaluated for significance using residual randomization permutation procedures as implemented in the *RRPP* R package (Collyer and Adams, 2018, 2019).

3.4. Annual growth increments

In *A. antiqua*, the relationship between external growth rings and the timing of their formation was studied through mark-recapture experiments (Clasing et al., 1994) and recently confirmed by stable isotope analysis (Boretto et al., 2019). These studies suggest that the external growth rings of *A. antiqua* form annually, providing a reliable means of determining ontogenetic age and estimating growth rate (Fig. 3).

For this study, 8 fossil and 8 modern shells were coated with epoxy resin to avoid shell fracture during sectioning. Then each shell was cross-sectioned (perpendicular to the growth lines) along the axis of maximum growth using a low-speed precision saw (Buehler Isomet), and polished using a 2-speed grinder-polisher (Buehler Alpha) with grits of 1200, 2500 and 4000 μm. These cross-sections (Fig. 3 A-B) allowed us to check the correspondence of internal growth lines with external rings. Ontogenetic ages were determined, and the maximum height of each of the annual growth rings ($L_{t+1} - L_t$) was measured using a digital calliper (precision of 0.01 mm) (Fig. 3C).

The use of annual growth increments allows the autocorrelation of successive measurements in the same individual to be reduced. Furthermore, individual growth increment profiles (as a function of shell size) provide more information on shell growth and variation patterns than cumulative growth curves (Escati-Peñaloza et al., 2010). Annual growth increments (fossil: $N = 36$, and modern: $N = 39$) were calculated as the difference between the maximum lengths of successive growth rings.

Following Escati-Peñaloza et al. (2010), the *A. antiqua* growth can be analyzed using the Chapman-Richards equation:

$$L_t = L_\infty \left(1 - e^{-k(t-t_0)}\right)^{1/(1-M)} \tag{1}$$

where L_t is the length at time t, L_∞ the asymptote of the function, representing the length of the organism (umbo to commissure), k is the growth coefficient in units of years^{-1}, M the curvature parameter, and t_0 the age at $L_t = 0$. This function has an inflexion point at length, where the growth rate is maximum. The annual increments can be expressed as a function of size:

$$L_{t+1} - L_t = L_\infty \left\{ 1 - e^{-K} \left[1 - \left(\frac{L_t}{L_\infty}\right)^{1-m} \right] \right\}^{\frac{1}{1-m}} - L_t \tag{2}$$

Individual and assemblage growth parameters were estimated at an individual level using nonlinear mixed-effects models, which express each parameter as a function of the assemblage parameter ("fixed
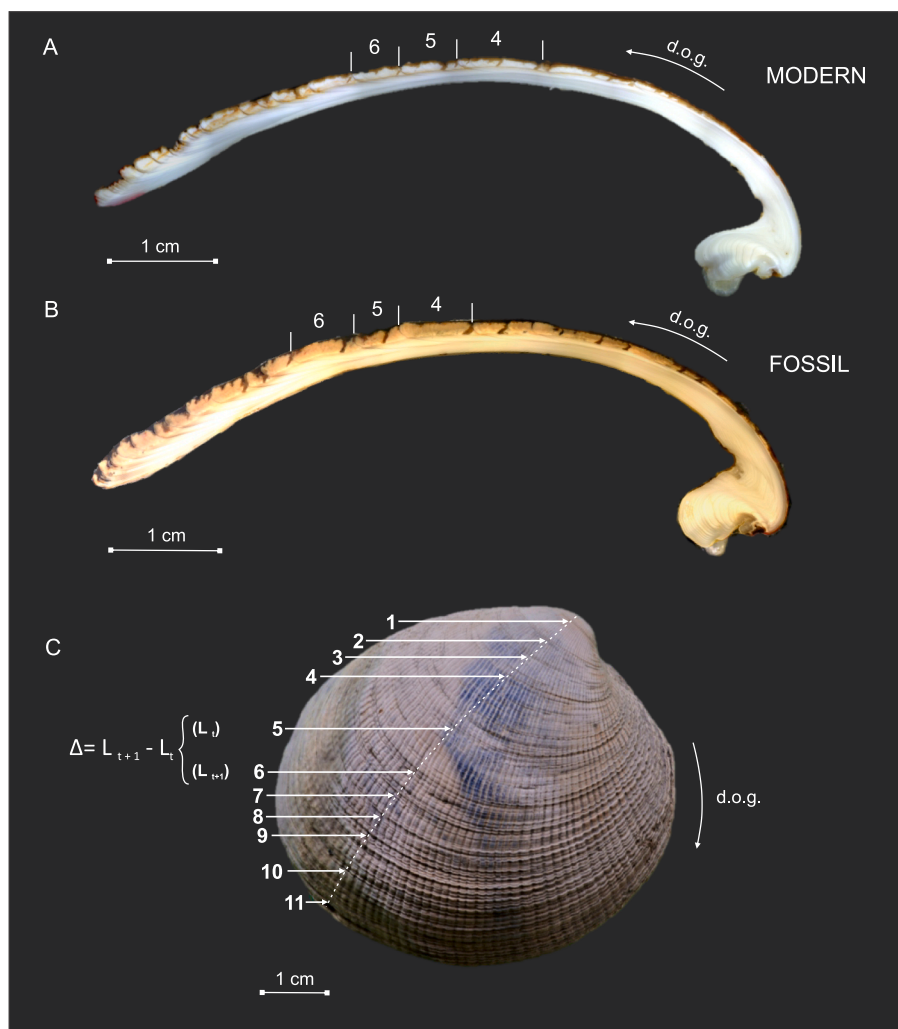
Fig. 3. Shell growth in *A. antiqua*. (A) Cross-section of a modern *A. antiqua* shell (ID #CB-A-06); (B) Cross-section of a fossil *A. antiqua* shell (ID #CB-H-08). Consecutive sampling from the outer shell layer in a cross-section is shown. (C) Shell exterior of *A. antiqua*, showing ontogenetic growth rings with annual increment. d.o.g.: direction of growth. Numbers give ontogenetic years within each shell specimen.

effect") and an individual deviation from these fixed effects ("random effect") (Lindstrom and Bates, 1990). The calculation of growth parameters through these models allows for the existing correlation in grouped data (per individual) to be incorporated into the analysis, which may be due to: (i) the variation in growth between individuals (random effects), and (ii) the autocorrelation due to variation within the same individual (random error).

Parameters were calculated using maximum likelihood methods implemented in the *nlme* R library (Pinheiro et al., 2007). Two nonlinear models were analysed: Model A, where variance increases as a power of the absolute value of the covariate (varPower function in *nlme* R package) and Model B, with the same variance structure as in A but an autoregressive correlation structure (corAR1 function in *nlme* R package). For model comparison and selection, the Akaike Information Criterion (AIC) and the Bayesian Information Criterion (BIC) were used, where the preferred model is the one with lowest AIC and BIC (Pinheiro et al., 2007). The parameters of the modern and fossil shells were compared using ANOVA between pairs of estimated parameters.

3.5. Preservation and stable isotope analysis ($\delta^{18}O$ & $\delta^{13}C$)

The radiocarbon-dated fossil shell (ID #CB-H-08) and one modern specimen (ID #CB-A-06) were used for stable oxygen ($\delta^{18}O$) and carbon ($\delta^{13}C$) isotope analysis. The state of preservation in the fossil shell specimen was verified by using confocal Raman microscopy (CRM; WITec alpha 300 R; c.f. Nehrke et al., 2012) at the Alfred Wegener Institute in Bremerhaven, Germany. The CRM setup was equipped with a diode laser (excitation wavelength 488 nm) and a 20× Zeiss objective. Both cross-sections dedicated to stable isotope analysis were checked by CRM spot measurements (14 spots in fossil and 12 spots in modern specimens) from the umbonal area to the ventral margin and at several arbitrary points in between. Shell material was milled from cross-sections (5 mm wide) (Fig. 3A-B) along the axes of maximum growth. Carbonate samples were collected from the outer shell layer using a 700 μm drill bit (Komet/Gebr. Brasseler GmbH & Co. KG) mounted onto an industrial high precision drill (Minimo C121, Minitor Co., Ltd.) and attached to a binocular microscope. Sample weight was approximately 40–60 μg. Milling was conducted in the direction of growth across the three ontogenetic years (i.e., increments) with maximum shell growth. To maximise comparability, increments milled in both cross-sections correspond to ontogenetic years four to six. Measurements were performed by isotope ratio mass spectrometry (IRMS) at the Alfred Wegener Institute for Polar and Marine Research (Bremerhaven, Germany) using a Thermo Finnigan MAT 253 coupled with an automated carbonate preparation device (Kiel IV). Measurements were calibrated against the international NBS-19 standard values of −4.28‰ and − 2.88‰ for $\delta^{18}O$ and $\delta^{13}C$ respectively. Results were reported in δ-notation and given as parts per mil (‰ Vienna Peedee belemnite [VPDB]). The long-term

precision based on an internal laboratory standard (Solnhofen limestone SHKBr2: −4.28‰; Solnhofenkalk Bremen Version 2) measured over 1 year together with samples was better than ±0.08‰ for stable oxygen isotopes and ± 0.06‰ for stable carbon isotopes.

Ratios of carbon isotopes (δ^{13}C) in marine bivalve species have been reported as potential future proxies (Beirne et al., 2012; Reynolds et al., 2017). However, as this proxy is not yet fully understood nor calibrated in *A. antiqua* shells, we report δ^{13}C data but do not discuss them in any climatic or environmental context.

3.6. Water temperatures derived from shell carbonate

For the reconstruction of water temperatures based on stable oxygen isotope ratios ($\delta^{18}O_{shell}$) of *A. antiqua* carbonate shells, the corrected palaeothermometry equation for aragonite of Grossman and Ku (1986) was used:

$$T(^{\circ}C) = 20.60 - 4.34 \left[\delta^{18}O_{shell} - (\delta^{18}O_{water} - 0.27) \right] \quad (3)$$

where T represents estimated temperature (°C), and $\delta^{18}O_{shell}$ and $\delta^{18}O_{water}$ refer to carbonate sample and water $\delta^{18}O$, respectively. The $\delta^{18}O_{water}$ ratio is expressed as the deviation from Vienna Standard Mean Ocean Water (VSMOW). Therefore, a 1‰ change in $\delta^{18}O_{shell}$ indicates a temperature change of 4.34 °C, if $\delta^{18}O_{water}$ remains unchanged.

Finding reliable $\delta^{18}O_{water}$ values for the BC area is one of the main challenges when using shell-derived stable oxygen isotope ratios for temperature reconstructions. We, therefore, follow the approach in Colonese et al. (2012) by using a range of $\delta^{18}O_{water}$ values instead of a single value. Using an average value of −1.2‰, a minimum value of −1.6‰ and a maximum value of −0.8‰, we can cover a certain variability in water chemistry along the BC and Golondrina Bay in particular. The value range in Colonese et al. (2012) is based on seven single $\delta^{18}O_{water}$ measurements in outer Cambaceres (CE) at Lanashuaia (white star symbol in Fig. 1) from December 2009 to October 2010. This range covers all the additional $\delta^{18}O_{water}$ measurements reported to our knowledge: −1.22 ± 0.19‰, which is the average value of 12 single measurements made monthly from October 2015 to October 2016 also at Lanashuaia, reported in Nicastro et al. (2020), and a single measurement taken at Ushuaia Bay of −1.6‰, reported in Obelic et al. (1998). Additionally, changes in ice volume over geological time have affected marine $\delta^{18}O_{water}$ values, which must be taken into account when comparing isotope-derived temperatures from fossil and modern specimens. Based on Fairbanks (1989) work and following Beierlein et al. (2015), we used a correction value of 0.0226‰. This correction enables comparability between fossil and modern $\delta^{18}O_{shell}$ derived measurements.

Rubo et al. (2018) report that *A. antiqua* does not form its shell in isotopic equilibrium with the ambient water. Since the offset of −0.9 ± 0.3‰ is reported as relatively constant throughout the lifetime, measurements of $\delta^{18}O_{shell}$ in this study were corrected for this offset before calculating water temperatures. Limitations to the climatic interpretation of our data are discussed in Section 5.1.

3.7. Instrumental data on water temperatures in the Beagle Channel

To have information on the annual temperature amplitude at the study site, we estimated a range from approximately 3 °C to 12 °C, which covers all the SST data reported in Colonese et al. (2012), for the outer Cambaceres Bay location, and Gordillo et al. (2015) and Nicastro et al. (2020) for Ushuaia Bay (4 km from the study area), which are the papers that provided the $\delta^{18}O_{water}$ measurements used in this paper.

4. Results

4.1. Shell dating

Radiocarbon data for the fossil shell from Cormoranes Archipelago yielded an age of 4300 ± 35 yr B.P (Poz-84995). The corresponding calibrated age is 3542 cal. yr B.P. (3444–3629 cal B.P. ±1σ).

4.2. Morphometric analysis

4.2.1. Linear morphometrics

A detailed summary of combined linear measurements in the fossil and modern shells is given in Table 1. In general, the fossil samples show higher values in all measurements than the modern samples.

ANOVA analysis performed on the values of each morphometric variable revealed significant differences between assemblages in terms of height (F = 6.78; p = 0.01), width (F = 16.38; p < 0.0001) and weight (F = 13.46; p < 0.0001) but not in length (F = 2.89; p = 0.09). Fossil shells were taller and heavier, with a wider umbo. The multivariate analysis of variance (MANOVA) performed on all measurements showed statistically significant differences (Wilks' lambda = 0.61; F = 8.59; p < 0.0001).

4.2.2. Geometric morphometrics

ANOVA analysis using RRPP on centroid sizes revealed that fossil shells were significantly larger than their modern counterparts (F = 5.28; Z = 3.41; p < 0.001) (Fig. 4). The ANCOVA design on shape co-ordinates revealed a significant effect of assemblages (modern/fossil) (p < 0.001; R^2 = 0.12), a non-significant effect of size on shape (p = 0.06; R^2 = 0.027), and a significant interaction term (period*centroid size) (p < 0.001) indicating differences in static allometry between periods. The comparison between vectors (fossil vs modern) showed that they are not parallel (p = 0.001; r = −0.72; angle = 135°).

Principal Component Analysis (PCA) (Fig. 4) differentiated fossil and modern shell shapes. The first three Principal Components (PC) accounted for 39.49%, 13.07% and 10.71% of the variation explained, respectively. The variation along PC1 indicates distinct intra-specific variation in both assemblages and overlap between them. This variation is mainly observed in landmarks (LM) 1 to 4, 11 and 12 and in the contour. The LM 1 to 4, i.e., the cardinal teeth, are more developed in the modern specimens. The LM 11 and 12 located at the tip of the posterior adductor muscle and at the end of the ligament, respectively, are more separated in the case of the fossil specimens, thus defining a shorter ligament in these cases than in the modern. Also, the semilandmark configuration makes it possible to visualize incipient dorsal *rostrum* in the contour of the fossil shells. The pallial sinus (LM 8–9-10) was more open in the modern shells.

4.3. Annual growth increments

Maximum and average ontogenetic age values, as well as average sizes for each assemblage, are shown in Table 2. In general, fossil shells

Table 1
Linear measurements performed on right modern and fossil shells of *A. antiqua* in the Beagle Channel. The number of specimens analysed (N), mean value, standard deviation (SD) and range for each measurement are shown.

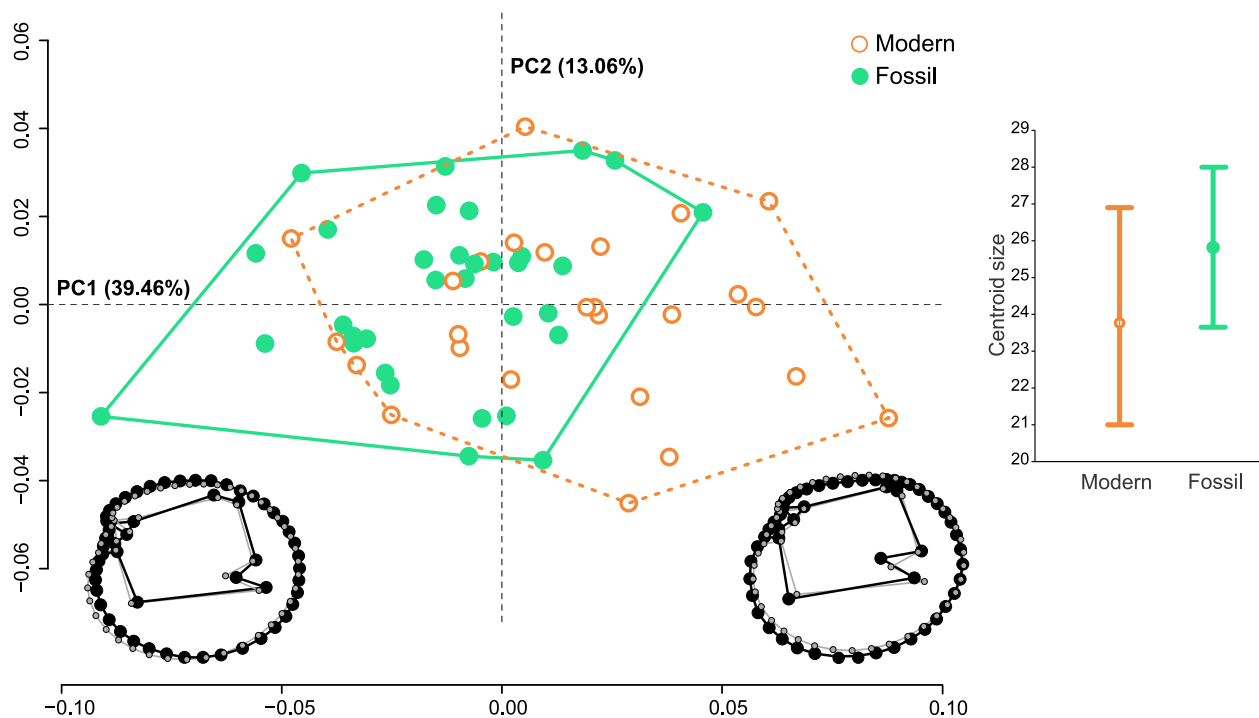|		Length (mm)	Height (mm)	Width (mm)	Weight (mg)
Modern	N	32	32	32	32
	$\overline{X} \pm$ SD	66.8 ± 1.4	57.2 ± 1.2	16.2 ± 0.4	21.7 ± 1.5
	Range	(49.9–80.1)	(42–68.4)	(12.2–21.4)	(8.2–44.6)
Fossil	N	28	28	28	28
	$\overline{X} \pm$ SD	69.9 ± 1	61.3 ± 1	19.5 ± 0.7	30.1 ± 1.7
	Range	(59.8–80.3)	(50.5–71.5)	(15.5–37.5)	(14.8–56.4)

Fig. 4. Principal component analysis (PCA, first and second) of the Procrustes coordinates of *A. antiqua* of fossil (green filled circles) and modern (empty orange circles) shells with respective percentages of variation explained. On the edges: graphic representations of the PC1 extreme configurations (black) and the consensus configuration in each case (grey). On the right: Mean (point) and standard deviation (whiskers) of fossil and modern centroid shell sizes. (For interpretation of the references to colour in this figure legend, the reader is referred to the web version of this article.)

Table 2

Ontogenetic age and average size (calculated through cumulative increment width) and standard deviation values of *A. antiqua* shells from the Beagle Channel.

	Height (mm)			Ontog. age			Min-Max Ontog. Age
	$\overline{X}$	SD	N	$\overline{X}$	SD	N	
Modern	57.4	7.6	31	13.2	2.0	39	[8–18]
Fossil	61.2	5.7	31	15.9	2.5	36	[11–21]

showed larger sizes and higher average ages than modern.

There is a similar pattern of annual growth increment widths in fossil and modern assemblages (Fig. 5). Annual growth increments increase until ontogenetic year four or five, which represents the inflexion point in growth. From there, increment widths begin to decrease until ontogenetic years 13–15, reaching minimum values afterwards (Fig. 5A-B). The total increment width range varied from 0.84–12.36 mm in modern shells and 0.73–12.07 mm in fossil shells.

4.3.1. Nonlinear mixed models

The comparison of fitted models showed that AIC and BIC values are higher as the complexity of the model increases. Model A showed lower values for both criteria (AIC = 4367.48, BIC = 4437.34) than model B (AIC = 4369.50, BIC = 4444.34). The autocorrelation between successive rings was low ($\rho = 0.2$). The semivariogram function was also used to test for autocorrelation, but no marked correlation between successive growth rings was found. As a result, Model A was chosen to represent the growth of the fossil and modern *A. antiqua* specimens.

Growth parameters calculated varied between fossil and modern shells (Fig. 6). Asymptotic length (L_∞) was higher for fossil than for modern shells, while the growth coefficient (k) and the curvature parameter (m) were higher for modern shells (Fig. 6). The statistical significance in fixed effects was assessed by the ANOVA function. Differences were found in L_∞ (F = 22.04, $p < 0.0001$), and m (F = 9.8; $p =$
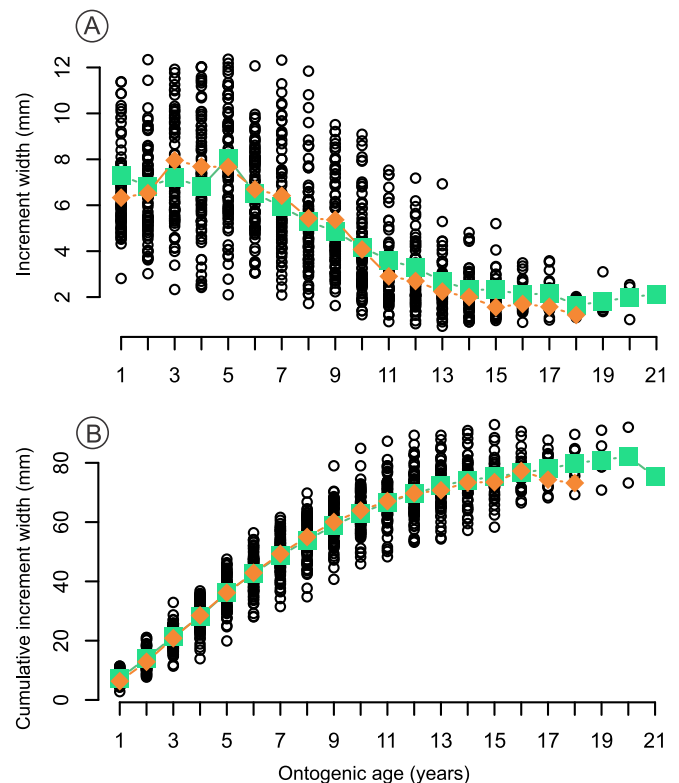

Fig. 5. Annual growth increment widths of fossil and modern *A. antiqua* specimens from the Beagle Channel. (A) Increment width vs ontogenetic age, (B) Cumulative growth width vs ontogenetic age. Means of fossil (green square symbols) and modern (orange diamond symbols) assemblages are shown. (For interpretation of the references to colour in this figure legend, the reader is referred to the web version of this article.)
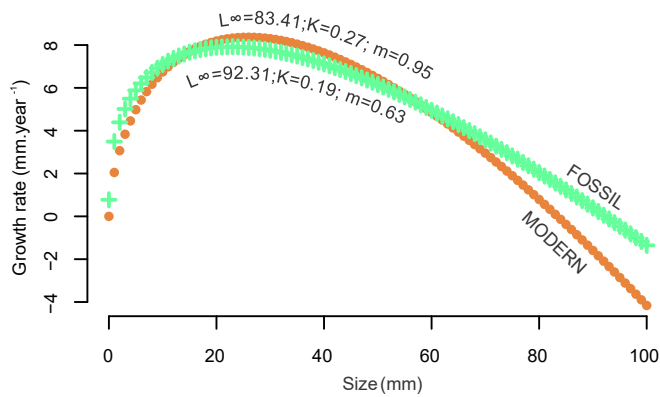
Fig. 6. Average growth rates predicted by Richards growth model (model A) for fossil (green cross symbols) and modern (orange filled circles) *A. antiqua* specimens from the Beagle Channel. (For interpretation of the references to colour in this figure legend, the reader is referred to the web version of this article.)

0.0018) but not in k (F = 0.015; p = 0.90).

4.4. Preservation and stable oxygen and carbon isotope analysis ($\delta^{18}O$ & $\delta^{13}C$)

The diagenetic check for alterations within the shells conducted by confocal Raman microscopy, applied on both the modern and fossil shells used for stable isotope analysis, confirmed that both shells consist entirely of pristine aragonite. All 26 Raman spectra showed characteristic peaks of aragonite at around 206 cm^{-1} and 1085 cm^{-1} (Fig. 7A).

For stable isotope analysis, we measured a total of 47 consecutive samples in the fossil and 42 consecutive samples in the modern shell specimen, covering ontogenetic years four to six. All the isotope profiles ($\delta^{18}O_{shell}$ and $\delta^{13}C_{shell}$) show, to some degree, a sinusoidal pattern, which, however, is more prominent in both $\delta^{18}O_{shell}$ profiles (Fig. 7 B, C). The average $\delta^{18}O_{shell}$ value in the modern shell is 0.62‰ and ranges from −0.25‰ to +1.43‰, while the average $\delta^{13}C_{shell}$ value is 1.50‰, ranging from +0.57‰ to +1.87‰. For the fossil shell, the average $\delta^{18}O_{shell}$ value is −0.37‰, ranging from −1.09‰ to +0.70‰. The average $\delta^{13}C_{shell}$ value of 0.63‰ ranges between +0.17‰ and + 1.04‰ (Fig. 7 B, C). Mean values of $\delta^{18}O_{shell}$ and $\delta^{13}C_{shell}$ show significant differences between the modern and the fossil shell (ANOVA $\delta^{18}O_{shell}$ F = 13.59; p < 0.0001; $\delta^{13}C_{shell}$ F = 24.41; p < 0.0001).

The $\delta^{18}O_{shell}$ profiles of both the fossil and the modern shell show similar sinusoidal patterns and a similar amplitude (Fig. 7 B, C). This pattern is consistent with observations for *A. antiqua* in Rubo et al. (2018) and Boretto et al. (2019).

4.5. Water temperatures derived from shell carbonate

After careful consideration and correction for global ice volume changes (in the fossil shell) and for the disequilibrium offset in *A. antiqua* shell carbonate, and using a range of $\delta^{18}O_{water}$ values, following Colonese et al. (2012), we were able to calculate water temperatures from the modern and the fossil shell specimens. Results are shown in Fig. 8. The modern shell gives an average value of 7.6 °C, ranging from 4.1 °C to 11.4 °C. The water temperatures for the fossil shell are about 4.4 °C higher than the modern one: the average value is 12.0 °C, ranging from 7.4 °C to 15.2 °C (all relative to using the average $\delta^{18}O_{water}$ value of −1.2‰).
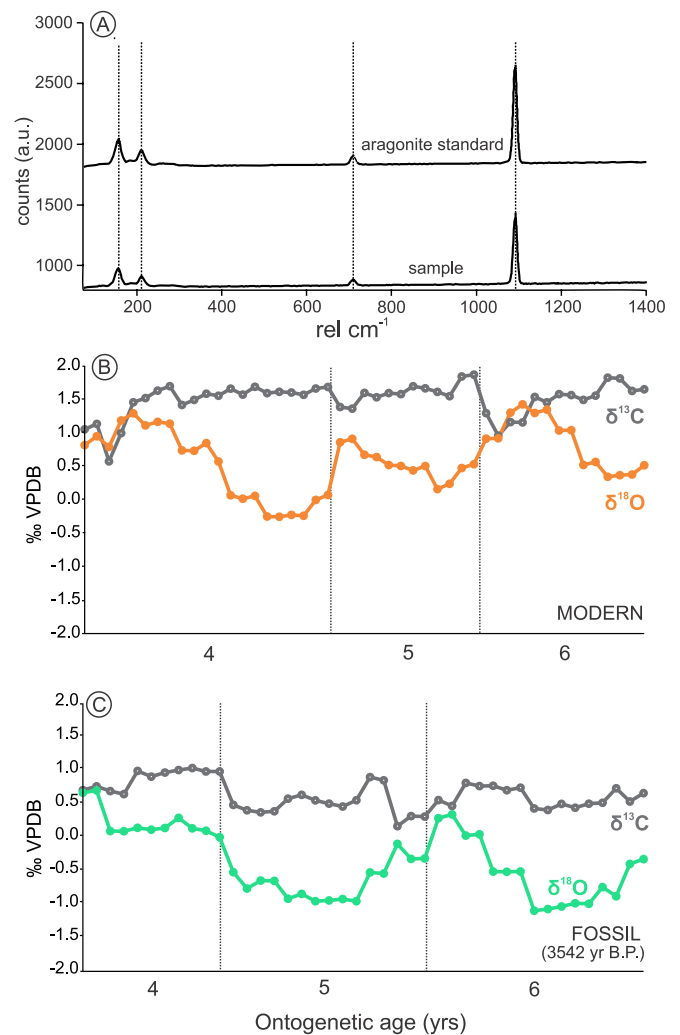

Fig. 7. (A) Confocal Raman spectrum of the fossil shell showing the characteristic peaks of aragonite at around 206 cm^{-1} and 1085 cm^{-1}. Stable isotope data derived from fossil and modern shell specimens. (B) Stable oxygen (orange) and stable carbon (grey) isotope profiles of the modern shell; (C) Stable oxygen (green) and stable carbon (grey) isotope profiles of the fossil shell. (For interpretation of the references to colour in this figure legend, the reader is referred to the web version of this article.)

5. Discussion

5.1. Evidence of warming in Late Holocene?

When estimating water temperatures from carbonate shells, there are several uncertainties and limitations to address. Firstly, it is necessary to be cautious with interpretations made from observing a single specimen, since there is a possibility that the differences observed are due to individual variability or microhabitat differences (i.e., changes in salinity, $\delta^{18}O_{water}$, etc.). Secondly, Rubo et al. (2018) reported that, based on the analysis of 17 specimens from San Jorge Gulf (Patagonia Argentina) *A. antiqua* does not form its shell in isotopic oxygen equilibrium with the aquatic environment, and this gives a negative offset of −0.9 ± 0.3‰. Although this offset was corrected mathematically in our study, the deviation may have some variability between specimens. Therefore, future studies must consider a greater number of specimens and more detailed isotopic signals ($\delta^{18}O_{shell}$) in *A. antiqua* shells from the BC (Mette et al., 2019). Lastly, the shell oxygen isotope-based palaeotemperatures estimated are challenging to interpret for the BC area. A common problem in determining temperatures in marine waters is that
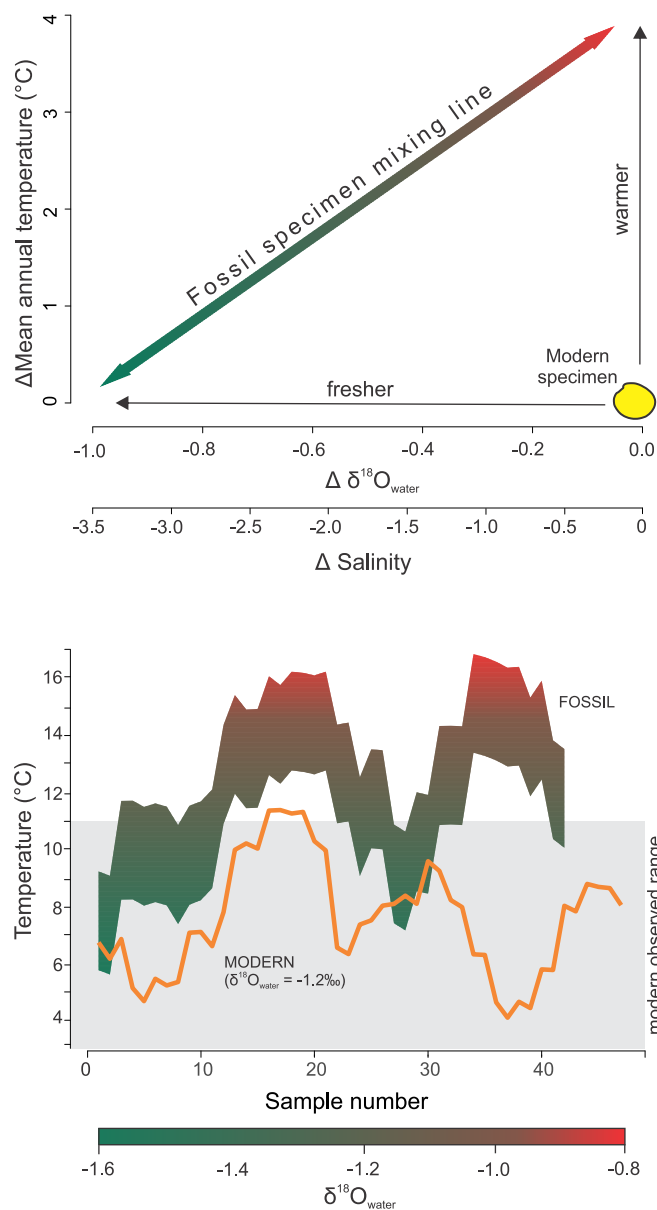
Fig. 8. (A) Mixing model between seawater composition and mean annual temperature of the *A. antiqua* fossil specimen. Values are expressed as deviations (Δ) from the modern specimen and range from no change in $\delta^{18}O_{water}$ (and a + 4.3 °C change in temperature) to no change in temperature (and a − 1‰ change in $\delta^{18}O_{water}$). The line between these two endmembers reflects all other possible combinations of the two variables that would yield the same $\delta^{18}O_{shell}$ value. ΔSalinity (second x-axis) was calculated using the linear relationship between $\delta^{18}O_{water}$ and salinity defined by Eq. 1 of Colonese et al. (2012). (B) Comparison of the modern seasonal temperature profile (assuming $\delta^{18}O_{water} = -1.2‰$) with the fossil data, under a range of $\delta^{18}O_{water}$ values. Modern observed range from outer Cambaceres Bay (Colonese et al., 2012).

some coastal waters are heavily influenced by freshwater (brackish water), which is generally depleted in ^{18}O (compared to open ocean waters). Depending on the degree of local freshwater mixing in coastal areas, the $^{18}O_{water}$ content may be consequently low, and then palaeotemperatures would be too high. Therefore, we have addressed the analysis and discussion considering these uncertainties.

The bivalve *A. antiqua* grows its shell mainly in summer but also in winter. It thus has the potential to record the entire annual temperature range within its shell carbonate (Rubo et al., 2018). Due to the lack of $\delta^{18}O_{water}$ measurements at the collection site, and as described in Section 3.6, we used an average $\delta^{18}O_{water}$ value of −1.2‰ to calculate water

temperatures (Fig. 8) and then compared the resulting value range to the temperature and SST data reported for the BC area (Section 3.7). As shown in Fig. 8, the estimated temperature based on the $\delta^{18}O_{shell}$ ratios covers the instrumental temperature range very well (grey area in Fig. 8A). This confirms that the *A. antiqua* shell records entirely or almost entirely the annual ambient temperature range.

Since the temperature reconstruction in the modern shell provided auspicious results, we calculated palaeotemperatures derived from the fossil shell specimen. After correcting for global sea ice changes over time (Section 3.6) and a test for diagenetic alterations within the shell carbonate (Section 4.4), we used the same $\delta^{18}O_{water}$ value range as for the modern shell. If we assume there was no difference in the $\delta^{18}O_{water}$ value between 3542 yr B.P. and the present time (c.f. Fig. 8B), the temperatures estimated for the fossil shell are considerably higher than for the modern shell: both winters and summers show warmer temperatures, with the average temperature being 4.4 °C higher in the fossil shell.

Considering the uncertainties mentioned above associated with our oxygen isotope data, we propose a spectrum of possible scenarios to discuss and interpret them. Fig. 8A refers to a mixing line for the fossil specimen, i.e. the range of possible combinations of $\delta^{18}O_{water}$ change and temperature that would produce the same $\delta^{18}O_{shell}$. Since linear relationships define all variables, we have used the changes compared to modern (Δ) (instead of absolute values). Given the existing relationship between $\delta^{18}O_{water}$ and salinity, we use Eq. 1 of Colonese et al. (2012) to convert $\Delta\delta^{18}O_{water}$ to Δsalinity on the second x-axis. Following the graph, in a scenario where salinity (and hence $\delta^{18}O_{water}$) does not change between past and present, the mean temperature would be +4.3 °C warmer at 3542 yr B.P. If, on the contrary, the mean temperature was the same, it would result in $\delta^{18}O_{water}$ being 1‰ lower (see Section 3.6). Within these two extremes, many combined scenarios are possible. Previous palaeoclimatic studies in the area provide clues that may help to explore them. On the one hand, our paleotemperatures lie within the palaeotemperature range of Gordillo et al. (2015), who reported a 6–18 °C temperature range for a 3839 yr B.P. *Retrotapes exalbidus* shell from the same fossil deposit as the present work (Cormoranes Archipelago, Fig. 1). In addition, our results match previous studies that report warming for the BC area between 4500 and 3000 yr B.P. (Panarello, 1987; Obelic et al., 1998; Gordillo et al., 2011, 2014). However, this evidence derives from oxygen isotopic data, which carries the same limitations on the $\delta^{18}O_{water}$ values in the BC. Studies carried out in the broader region exploring other proxies and methodologies describe this climate optimum, although there are still many uncertainties about its intensity (see Pendall et al., 2001; Nielsen et al., 2004; Renssen et al., 2005; Etourneau et al., 2013). In addition, evidence based on the diversification of molluscan taxa supports the hypothesis that there was a climatic optimum around 4000 yr B.P. in the BC with the expansion of several calcareous taxa (Gordillo et al., 2005; Gordillo, 2009; Gordillo, 2013). Also, palynological studies in Río Ovando (Cormoranes Archipelago) in deposits from 4000 to 3000 yr B.P. register cold-water dinocyst assemblages, typical of marginal marine environments used as an indicator of warm waters in polar and sub-polar zones (Candel et al., 2009, 2018). However, previous studies also support a salinity change scenario for the BC. The palynological evidence shows species typical of low to moderate salinity waters in the Cormoranes Archipelago about 3500 yr B.P. (Candel et al., 2009). While at present, the BC waters are influenced by strong freshwater discharge from rainfall and glacier meltwater through rivers (Isla et al., 1999), the comparison of modern and fossil (between 4000 and 3500 yr B.P.) palynological assemblages from the Cormoranes Archipelago area suggests that a high fluvial input took place in the past (Candel et al., 2009, 2013). At this point, it is essential to determine whether a difference in salinity in the waters of the Cormoranes Archipelago may also be a consequence of factors associated with its geomorphology, which differs from a coastline such as Bahía Golondrina. Candel et al. (2013) conducted palynological comparisons of 22 sites along the BC, including bays, which

could be considered analogous to the environment in the Cormoranes Archipelago near 3500 yr B.P. The sites show similar signs of freshwater input in all cases, suggesting similar salinity variability in all environments. Also, malacological evidence indicates that the fossil species composition deposits in the Cormoranes Archipelago are typical of a marine environment, similar to that currently found in the BC (Gordillo, 1999), suggesting similarities in environmental characteristics between the two sites (Cormoranes Archipelgo and Golondrina Bay).

Our results of the shell growth pattern and size (both linear measurements and centroid size) are compatible with a freshwater input for 3542 yr B.P. Fossil shell specimens are larger (both in width and height), heavier, with greater maximum length, with a more pronounced umbo, and are more long-lived than modern specimens. However, no significant differences were found in the growth coefficient (k) between assemblages. According to Saulsbury et al. (2019), if organisms with similar k but different L_{∞} values are compared, those with higher L_{∞} values would secrete more shell in terms of length per time. Several studies have shown that growth is consistent with the months of higher productivity and thus that the growth of *A. antiqua* is highly dependent on food availability (Clasing et al., 1994; Stead et al., 1997; Lazareth et al., 2006; Escati-Peñaloza et al., 2010; Riascos et al., 2012; Rubo et al., 2018). Some authors have posited that the high fluvial input into the marine environment reported for 4000–3500 yr B.P. would cause an elevated entry of sediments and terrestrial material into the BC, increasing primary productivity (Candel et al., 2009; Gordillo et al., 2015). These conditions may have promoted growth in fossil clams, reflected not only in the shells but also in the umbo's width. Also, the longevity observed in fossil shells appears to be a response to this increase in primary productivity. It is likely that, by reaching larger sizes earlier, especially during the first years of life, this operates as a protective factor against predators (Haveles and Ivany, 2010; Ridgway et al., 2011). Considering the results found in shell shape, characteristics such as an elongated shape (useful for a quick and efficient burial) (Stanley, 1970) may also have contributed to the increase of lifespan. Gordillo et al. (2013) suggested that around 4000 cal. yr B.P., as a result of changes in salinity, mass mortality occurred in the area, mainly in filter clams, changing the relationship between filter feeders and predators. This event could have resulted in higher predation pressure and would explain the elongated contour and the presence of the dorsal *rostrum* in the fossil shells of *A. antiqua*.

Our isotope results do not provide sufficient evidence to confirm nor deny a + 4.4 °C warming hypothesis for the Late Holocene, even though other proxies indicate higher productivity in the 3542 yr B.P. waters, which may indirectly be linked to a warm moment and ice melting. Previous studies suggest that a salinity change took place at that time (Candel et al., 2009; Gordillo, 2013), which, in our case, would result in an overestimation of the calculated palaeotemperatures. Seemingly, this salinity change was rather moderate. This assumption is based on the analyses of palynological and malacological assemblages in the area which show only slight changes when compared to stages of high saline variability (Candel et al., 2009, 2013, 2018; Gordillo et al., 2005; Gordillo, 2009). Further studies, including higher numbers of specimens, more isotopic data and hence, a detailed calibration of *A. antiqua* $\delta^{18}O_{shell}$ values, are needed. To obtain absolute palaeotemperatures, independent of seawater chemistry, future analysis should consider including carbonate clumped isotope thermometry, as this is a promising alternative proxy of palaeotemperatures in bivalve shells (Henkes et al., 2018; Caldarescu et al., 2021).

5.2. Changing habitat energy

According to previous geomorphological and palaeontological studies (Rabassa et al., 1986; Gordillo et al., 1993; Gordillo et al., 2005; Rabassa et al., 2009), the sampling area of the fossil specimens (Cormoranes Archipelago Fig. 1) was affected by a complex environmental evolution (described in section 2.2) (see details in Fig. 2 in Gordillo

et al., 1993). As a result, individuals of *A. antiqua* from the Lapataia and Ovando rivers would have lived in a marine archipelago environment. This habitat would be less energetic than the current beach in Golondrina Bay, which has a coast open to the BC, with more exposure to waves and tides. Since *A. antiqua* has a quasi-circular shaped shell and is a superficial or shallow burial species (Urban and Campos, 1994), high-energy habitats would result in greater vulnerability to sources of physical disturbance, such as storms, wave action, etc. These environmental conditions may also have contributed to the increase in longevity observed in fossil specimens.

Shell shape may reflect the environmental differences described above. In high energy habitats, such as Golondrina Bay, where storm events repeatedly occur, clams can be removed from their semi-infaunal or infaunal life positions, transported and deposited outside the sediment (Neubauer et al., 2013). In this scenario, clams require a greater degree of mechanical stability; hence they adopt a hydrodynamically more stable horizontal orientation (Kondo, 1987; Gordillo and Archuby, 2014). In *A. antiqua*, both cardinal teeth and ligament are the primary opponents of stress due to lateral displacement of the shells, and muscles operate in closing them. In this study, we found that the ligament and the cardinal teeth in modern shells are more developed than in fossil shells (Fig. 4). These differences may be related to improving mechanical stability in a more energetic current environment than in the past. This trend coincides with the shell shape changes over time observed in *A. antiqua* from northern Patagonia in response to changes in habitat energy (San Matías Gulf; Morán et al., 2018).

6. Conclusions

The present study highlights the importance of multi-proxy approaches to strengthen interpretations related to palaeoclimatic and palaeoenvironmental reconstructions, which allowed us to detect the adaptations and changes that occur in *A. antiqua* shells from the BC. Although the present work shows the climatic and environmental signals that are archived in *A. antiqua* shells, which can be interpreted locally and regionally, further research is essential to achieve a more comprehensive palaeoclimatic and palaeoenvironmental reconstruction for the southern tip of South America. The results obtained from the approaches performed show:

-Modern $\delta^{18}O_{shell}$ ratios in *A. antiqua* result in temperature estimates that cover the entire seasonal temperature range for the BC. A warming is shown by the reconstructed palaeotemperatures from a 3542 yr B.P. shell specimen, assuming no change in $\delta^{18}O_{water}$ (and therefore no change in salinity) in the BC.

- Part of the estimated water temperature differences between the fossil and modern shell could be due to the low salinity caused by the freshwater input reported for 4000–3500 yr B.P. into the BC, resulting in lower $\delta^{18}O_{water}$ values;

- Greater growth, size and longevity in fossil specimens was likely enabled by increasing primary productivity in the area due to a greater contribution of sediments and terrestrial material to the BC;

-A low-energy environment typical of a marine archipelago is reflected in the smaller ligaments, cardinal teeth and pallial sinus in the fossil specimens.

Declaration of Competing Interest

None.

Appendix A. Supplementary data

Supplementary data to this article can be found online at https://doi.org/10.1016/j.palaeo.2021.110574.

References

Adams, D., Rohlf, F.J., Slice, D.E., 2004. Geometric morphometrics: ten years of progress following the revolution. Ital. J. Zool. 71, 5–16. https://doi.org/10.1080/11250000409356545.

Adams, D., Collyer, M., Kaliontzopoulou, A., 2020. Geomorph: Software for geometric morphometric analyses. R Package Version 3 (2), 1.

Aguirre, G.E., Capitanio, F.L., Lovrich, G.A., Esnal, G.B., 2012. Seasonal variability of metazooplankton in coastal sub-Antarctic waters (Beagle Channel). Mar. Biol. Res. 8 (4), 341–353. https://doi.org/10.1080/17451000.2011.627922.

Almandoz, G.O., Hernando, M.P., Ferreyra, G.A., Schloss, I.R., Ferrario, M.E., 2011. Seasonal phytoplankton dynamics in extreme southern South America (Beagle Channel, Argentina). J. Sea Res. 66 (2), 47–57. https://doi.org/10.1016/j.seares.2011.03.005.

Balech, E., Ehrlich, M.D., 2008. Esquema biogeográfico del mar Argentino. Revista de Investigación y Desarrollo Pesquero 19, 45–75.

Beierlein, L., Salvigsen, O., Schöne, B.R., Mackensen, A., Brey, T., 2015. The seasonal water temperature cycle in the Arctic Dicksonfjord (Svalbard) during the Holocene Climate Optimum derived from subfossil *Arctica islandica* shells. The Holocene 25 (8), 1197–1207. https://doi.org/10.1177/0959683615580861.

Beirne, E.C., Wanamaker, A.D., Feindel, S.C., 2012. Experimental validation of environmental controls on the δ13C of Arctica islandica (ocean quahog) shell carbonate. Geochim. Cosmochim. Acta 84 (0016–7037), 395–409. https://doi.org/10.1016/j.gca.2012.01.021.

Bookstein, F.L., 1997. Morphometric Tools for Landmark Data: Geometry and Biology. Cambridge University Press.

Boretto, G.M., Gordillo, S., Cioccale, M., Colombo, F., Fucks, E., 2013. Multi-proxy evidence of Late Quaternary environmental changes in the coastal area of Puerto Lobos (northern Patagonia, Argentina). Quat. Int. 305, 188–205. https://doi.org/10.1016/j.quaint.2013.02.017.

Boretto, G.M., Baranzelli, M.C., Gordillo, S., Consoloni, I., Zanchetta, G., Morán, G., 2014. Shell morphometric variations in a Patagonian Argentina clam (*Ameghinomya antiqua*) from the Mid-Pleistocene (MIS 7) to the present. Quat. Int. 352, 48–58. https://doi.org/10.1016/j.quaint.2014.09.033.

Boretto, G., Consoloni, I., Morán, G.A., Regattieri, E., Gordillo, S., Fucks, E., Zanchetta, G., Dallai, L., 2019. Oxygen stable isotope analyses on *Ameghinomya antiqua* shells: a promising tool for palaeoenvironmental reconstruction along the Quaternary Patagonian Argentina coast? Alpine Mediterr. Quater. 32 (1), 1–16. https://doi.org/10.26382/AMQ.2019.06.

Bujalesky, G., 2007. Coastal geomorphology and evolution of Tierra del Fuego (Southern Argentina). Geol. Acta 5, 337–362.

Bujalesky, G.G., Coronato, A.M., Rabassa, J.O., Acevedo, R.D., 2008. El Canal Beagle. Un ambiente esculpido por el hielo. In: Ardolino, A., Lema, H. (Eds.), Sitios de Interés Geológico de la República Argentina, SEGEMAR, Anales, vol. 46, 2, pp. 849–864 (Buenos Aires).

Bujalesky, G.G., Isla, F.I., Montes, A., 2021. Differential Uplifting Rates Across the Magellan Fault: Interactions Between South American and Scotia Plates. Geol. Res. Tierra Del Fuego 289.

Butler, P.G., Schöne, B.R., 2017. New research in the methods and applications of sclerochronology. Palaeogeogr. Palaeoclimatol. Palaeoecol. 465, 295–299. https://doi.org/10.1016/j.palaeo.2016.11.013.

Caldarescu, D.E., Sadatzki, H., Andersson, C., Schäfer, P., Fortunato, H., Meckler, A.N., 2021. Clumped isotope thermometry in bivalve shells: A tool for reconstructing seasonal upwelling. Geochim. Cosmochim. Acta 294, 174–191. https://doi.org/10.1016/j.gca.2020.11.019.

Candel, M.S., Borromei, A.M., Martínez, M.A., Gordillo, S., Quattrocchio, M., Rabassa, J., 2009. Middle–Late Holocene palynology and marine mollusks from Archipiélago Cormoranes area, Beagle Channel, southern Tierra del Fuego, Argentina. Palaeogeogr. Palaeoclimatol. Palaeoecol. 273 (1–2), 111–122. https://doi.org/10.1016/j.palaeo.2008.12.009.

Candel, M.S., Borromei, A.M., Martínez, M.A., Bujalesky, G., 2013. Palynofacies analysis of surface sediments from the Beagle Channel and its application as modern analogues for Holocene records of Tierra del Fuego, Argentina. Palynology 37, 62–76. https://doi.org/10.1080/01916122.2012.718994.

Candel, M.S., Borromei, A.M., Louwye, S., 2018. Early to middle Holocene palaeoenvironmental reconstruction of the Beagle Channel (southernmost Argentina) based on terrestrial and marine palynomorphs. Boreas 47, 1072–1083. https://doi.org/10.1111/bor.12322.

Castellanos, Z., 1967. Catálogo de los Moluscos marinos Bonaerenses. Comisión De Investigaciones Científicas, La Plata. 8, 1–365.

Clasing, E., Brey, T., Stead, R., Navarro, J., Asencio, G., 1994. Population dynamics of *Venus antiqua* (Bivalvia: Veneracea) in the Bahía de Yaldad, Isla de Chiloé, southern Chile. J. Exp. Mar. Biol. Ecol. 177 (2), 171–186. https://doi.org/10.1016/0022-0981(94)90235-6.

Collyer, M.L., Adams, D.C., 2018. RRPP: An r package for fitting linear models to high-dimensional data using residual randomization. Methods Ecol. Evol. 9, 1772–1779. https://doi.org/10.1111/2041-210X.13029.

Collyer, M.L., Adams, D.C., 2019. RRPP: linear model evaluation with randomized residuals in a permutation procedure. R package version 0.4. 0.

Colonese, A.C., Verdún-Castelló, E., Álvarez, M., i Godino, I. B., Zurro, D., and Salvatelli, L., 2012. Oxygen isotopic composition of limpet shells from the Beagle Channel: implications for seasonal studies in shell middens of Tierra del Fuego. J. Archaeol. Sci. 39 (6), 1738–1748.

Constable, A.J., Melbourne-Thomas, J., Corney, S.P., Arrigo, K.R., Barbraud, C., Barnes, D.K.A., Bindoff, N.L., Boyd, P.W., Brandt, A., Costa, D.P., Davidson, A.T., Ducklow, H.W., Emmerson, L., Fukuchi, M., Gutt, J., Hindell, M.A., Hofmann, E.E., Hosie, G.W., Iida, T., Jacob, S., Johnston, N.M., Kawaguchi, S., Kokubun, N., Koubbi, P., Lea, M.-A., Makhado, A., Massom, R.A., Meiners, K., Meredith, M.P., Murphy, E.J., Nicol, S., Reid, K., Richerson, K., Riddle, M.J., Rintoul, S.R., Smith Jr., W.O., Southwell, C., Stark, J.S., Sumner, M., Swadling, K.M., Takahashi, K. T., Trathan, P.N., Welsford, D.C., Weimerskirch, H., Westwood, K.J., Wienecke, B.C., Wolf-Gladrow, D., Wright, S.W., Xavier, J.C., Ziegler, P., 2014. Climate change and Southern Ocean ecosystems I: how changes in physical habitats directly affect marine biota. Glob. Chang. Biol. 20, 3004–3025. https://doi.org/10.1111/gcb.12623.

Dietl, G.P., Kidwell, S.M., Brenner, M., Burney, D.A., Flessa, K.W., Jackson, S.T., Koch, P. L., 2015. Conservation palaeobiology: leveraging knowledge of the past to inform conservation and restoration. Annu. Rev. Earth Planet. Sci. 43, 79–103. https://doi.org/10.1146/annurev-earth-040610-133349.

Dietl, G.P., Smith, J.A., Durham, S.R., 2019. Discounting the past: the undervaluing of palaeontological data in conservation science. Front. Ecol. Evol. 7, 108. https://doi.org/10.3389/fevo.2019.00108.

Escati-Peñaloza, G., Parma, A.M., Orensanz, J.L., 2010. Analysis of longitudinal growth increment data using mixed-effects models: individual and spatial variability in a clam. Fish. Res. 105 (2), 91–101. https://doi.org/10.1016/j.fishres.2010.03.007.

Etourneau, J., Collins, L.G., Willmott, V., Kim, J.H., Barbara, L., Leventer, A., Schouten, S., Sinninghe Damsté, J.S., Bianchini, A., Klein, V., Crosta, X., Massé, G., 2013. Holocene climate variations in the western Antarctic Peninsula: evidence for sea ice extent predominantly controlled by insolation and ENSO variability changes. Clim. Past Discuss. 9 (1), 1–41. https://doi.org/10.5194/cp-9-1431-2013.

Fairbanks, R.G., 1989. A 17,000-year glacio-eustatic sea level record: influence of glacial melting rates on the Younger Dryas event and deep-ocean circulation. Nature 342, 637–642. https://doi.org/10.1038/342637a0.

Feruglio, E., 1950. Descripción geológica de la Patagonia, vol. 3. Dirección General de Y. P.F, Buenos Aires, 431 pp.

Franco, B.C., Combes, V., González Carman, V., 2020. Subsurface ocean warming hotspots and potential impacts on marine species: the southwest South Atlantic Ocean case study. Front. Mar. Sci. 7, 824. https://doi.org/10.3389/fmars.2020.563394.

Gillikin, D.P., Wanamaker, A.D., Andrus, C.F.T., 2019. Chemical sclerochronology. Chem. Geol. 526 (5), 1–6. https://doi.org/10.1016/j.chemgeo.2019.06.016.

Gordillo, S., 1999. Holocene molluscan assemblages in the Magellan region. Sci. Mar. 63 (S1), 15–22. https://doi.org/10.3989/scimar.1999.63s115.

Gordillo, S., 2009. Quaternary marine mollusks in Tierra del Fuego: insights from integrated taphonomic and palaeoecologic analysis of shell assemblages in raised deposits. Anales del Instituto de la Patagonia 37 (2), 5–16. https://doi.org/10.4067/S0718-686X2009000200001.

Gordillo, S., 2013. Cannibalism in Holocene muricid snails in the Beagle Channel, at the extreme southern tip of South America: an opportunistic response? Palaeontol. Electron. 16 (1), 4A, p13.

Gordillo, S., Archuby, F., 2014. Live-live and live-dead interactions in marine death assemblages: the case of the Patagonian clam *Venus antiqua*. Acta Palaeontol. Pol. 59 (2), 429–442. https://doi.org/10.4202/app.2011.0176.

Gordillo, S., Isla, F.I., 2011. Faunistic changes between the Middle/Late Pleistocene and the Holocene on the Atlantic coast of Tierra del Fuego: molluscan evidence. Quat. Int. 233 (2), 101–112. https://doi.org/10.1016/j.quaint.2010.06.006.

Gordillo, S., Bujalesky, G.G., Pirazzoli, P.A., Rabassa, J.O., Saliège, J.F., 1992. Holocene raised beaches along the northern coast of the Beagle Channel, Tierra del Fuego,

Argentina. Palaeogeogr. Palaeoclimatol. Palaeoecol. 99 (1–2), 41–54. https://doi.org/10.1016/0031-0182(92)90006-Q.

Gordillo, S., Coronato, A.M.J., Rabassa, J.O., 1993. Late Quaternary evolution of a subantarctic paleofjord, Tierra del Fuego. Quat. Sci. Rev. 12, 889–897. https://doi.org/10.1016/0277-3791(93)90027-J.

Gordillo, S., Coronato, A.M.J., Rabassa, J.O., 2005. Quaternary molluscan faunas from the island of Tierra del Fuego after the Last Glacial Maximum. Sci. Mar. 69 (S2), 337–348. https://doi.org/10.3989/scimar.2005.69s2337.

Gordillo, S., Martinelli, J., Cárdenas, J., Bayer, M.S., 2011. Testing ecological and environmental changes during the last 6000 years: a multiproxy approach based on the bivalve Tawera gayi from southern South America. J. Mar. Biol. Assoc. U. K. 91, 1413–1427. https://doi.org/10.1017/s0025315410002183.

Gordillo, S., Bernasconi, E., Cusminsky, G., Coronato, A.J., Rabassa, J.O., 2013. Late Quaternary environmental changes in southernmost South America reflected in marine calcareous macro-and-microfossils. Quat. Int. 305, 149–162. https://doi.org/10.1016/j.quaint.2012.11.016.

Gordillo, S., Bayer, M.S., Boretto, G., Charó, M., 2014. Mollusk shells as bio-geo-archives: Evaluating environmental changes during the Quaternary. In: Series: Springer Briefs in Earth System Sciences, 80 p.

Gordillo, S., Brey, T., Beyer, K., Lomovasky, B.J., 2015. Climatic and environmental changes during the middle to late Holocene in southern South America: A sclerochronological approach using the bivalve Retrotapes exalbidus (Dillwyn) from the Beagle Channel. Quat. Int. 377, 83–90. https://doi.org/10.1016/j.quaint.2014.12.036.

Grossman, E.L., Ku, T.L., 1986. Oxygen and carbon isotope fractionation in biogenic aragonite: temperature effects. Chem. Geol. (Isotope Geoscience Section) 59, 59–74. https://doi.org/10.1016/0168-9622(86)90057-6.

Harley, C.D., Randall, H.A., Hultgren, K.M., Miner, B.G., Sorte, C.J., Thornber, C.S., Rodriguez, L.F., Tomanek, L., Williams, S.L., 2006. The impacts of climate change in coastal marine systems. Ecol. Lett. 9 (2), 228–241. https://doi.org/10.1111/j.1461-0248.2005.00871.x.

Haveles, A.W., Ivany, L.C., 2010. Rapid growth explains large size of mollusks in the Eocene Gosport Sand, United States Gulf Coast. Palaios 25 (9), 550–564. https://doi.org/10.2110/palo.2009.p09-148r.

Henkes, G.A., Passey, B.H., Grossman, E.L., Shenton, B.J., Yancey, T.E., Pérez-Huerta, A., 2018. Temperature evolution and the oxygen isotope composition of Phanerozoic oceans from carbonate clumped isotope thermometry. Earth Planet. Sci. Lett. 490, 40–50. https://doi.org/10.1016/j.epsl.2018.02.001.

Hillebrand, H., Brey, T., Gutt, J., Hagen, W., Metfies, K., Meyer, B., Lewandowska, A., 2018. Climate change: Warming impacts on marine biodiversity. In: Handbook on marine environment protection. Springer, Cham, pp. 353–373.

IPCC, 2014. In: Core Writing Team, Pachauri, R.K., Meyer, L.A. (Eds.), Climate Change 2014: Synthesis Report. Contribution of Working Groups I, II and III to the Fifth Assessment Report of the Intergovernmental Panel on Climate Change. IPCC, Geneva, Switzerland, 151 pp.

Isla, F., Bujalesky, G., Coronato, A., 1999. Procesos estuarinos en el canal Beagle, Tierra del Fuego. Rev. Asoc. Geol. Argent. 54 (4), 307–318.

Kondo, Y., 1987. Burrowing depth of infaunal bivalves: observation of living species and its relation to shell morphology. In: Transactions and proceedings of the Paleontological Society of Japan. New series. Palaeontological Society of Japan, 148, pp. 306–323. https://doi.org/10.14825/prpsj1951.1987.148_306.

Lamy, F., Rühlemann, C., Hebbeln, D., Wefer, G., 2002. High–and low-latitude climate control on the position of the southern Perú-Chile Current during the Holocene. Paleoceanogr. Paleoclimatol. 17 (2), 1028. https://doi.org/10.1029/2001PA000727.

Lamy, F., Kilian, R., Arz, H.W., Francois, J.P., Kaiser, J., Prange, M., Steinke, T., 2010. Holocene changes in the position and intensity of the southern westerly wind belt. Nat. Geosci. 3 (10), 695–699. https://doi.org/10.1038/ngeo959.

Lardies, M.A., Clasing, E., Navarro, J.M., Stead, R.A., 2001. Effects of environmental variables on burial depth of two infaunal bivalves inhabiting a tidal flat in southern Chile. Marine Biological Association of the United Kingdom. J. Mar. Biol. Assoc. U. K. 81 (5), 809. https://doi.org/10.1017/S0025315401004635.

Lazareth, C.E., Lasne, G., Ortlieb, L., 2006. Growth anomalies in Protothaca thaca (Mollusca, Veneridae) shells as markers of ENSO conditions. Clim. Res. 30 (3), 263–269. https://doi.org/10.3354/cr030263.

Lindstrom, M.J., Bates, D.M., 1990. Nonlinear mixed effects models for repeated measures data. Biometrics 673–687.

Lockwood, R., Mann, R., 2019. A conservation palaeobiological perspective on Chesapeake Bay oysters. Philos. Trans. R. Soc. B 374 (1788), 20190209. https://doi.org/10.1098/rstb.2019.0209.

Mette, M.J., Whitney, N.M., Ballew, J., Wanamaker Jr., A.D., 2019. Reprint of Unexpected isotopic variability in biogenic aragonite: A user issue or proxy problem? Chem. Geol. 526, 84–92. https://doi.org/10.1016/j.chemgeo.2018.05.017.

Morán, G.A., Martínez, J.J., Boretto, G.M., Gordillo, S., Boidi, F.J., 2018. Shell morphometric variation of Ameghinomya antiqua (Mollusca, Bivalvia) during the late quaternary reflects environmental changes in North Patagonia, Argentina. Quat. Int. 490, 43–49. https://doi.org/10.1016/j.quaint.2018.05.027.

Nehrke, G., Poigner, H., Wilhelms-Dick, D., Brey, T., Abele, D., 2012. Coexistence of three calcium carbonate polymorphs in the shell of the Antarctic clam Laternula elliptica. Geochem. Geophys. Geosyst. 13, Q05014 https://doi.org/10.1029/2011GC003996.

Neubauer, T.A., Harzhauser, M., Mandic, O., 2013. Phenotypic evolution in a venerid bivalve species lineage from the late Middle Miocene Central Paratethys Sea: a multi-approach morphometric analysis. Biol. J. Linn. Soc. 110 (2), 320–334. https://doi.org/10.1111/bij.12120.

Nicastro, A., Surge, D., Godino, I.B., Álvarez, M., Schöne, B.R., Bas, M., 2020. High-resolution records of growth temperature and life history of two Nacella limpet species, Tierra del Fuego, Argentina. Palaeogeogr. Palaeoclimatol. Palaeoecol. 540, 109526. https://doi.org/10.1016/j.palaeo.2019.109526.

Nielsen, S.H., Koç, N., Crosta, X., 2004. Holocene climate in the Atlantic sector of the Southern Ocean: controlled by insolation or oceanic circulation? Geology 32 (4), 317–320.

Obelic, B., Álvarez, A., Argullós, J., Piana, E.L., 1998. Determination of water palaeotemperature in the Beagle Channel (Argentina) during the last 6000 yr through stable isotope composition of Mytilus edulis shells. Quater. South Am. Antarctic Peninsula 11, 47–71.

Panarello, H., 1987. Oxygen-18 temperatures on present and fossil invertebrate shells from Túnel Site, Beagle Channel, Argentina. Quater. South Am. Antarctic Peninsula 5, 83–92.

Peharda, M., Schöne, B.R., Black, B.A., Corrège, T., 2021. Advances of sclerochronology research in the last decade. Palaeogeogr. Palaeoclimatol. Palaeoecol. 570, 110371. https://doi.org/10.1016/j.palaeo.2021.110371.

Pendall, E., Markgraf, V., White, J.W.C., Dreier, M., Kenny, R., 2001. Multiproxy record of late Pleistocene–Holocene climate and vegetation changes from a peat bog in Patagonia. Quat. Res. 55, 168–178. https://doi.org/10.1006/qres.2000.2206.

Pinheiro, J., Bates, D., DebRoy, S., Sarkar, D., Team, R.C., 2007. Linear and nonlinear mixed effects models. R Package Version 3 (57), 1–89.

Poloczanska, E.S., Burrows, M.T., Brown, C.J., García Molinos, J., Halpern, B.S., Hoegh-Guldberg, O., Kappel, C.V., Moore, P.J., Richardson, A.J., Schoeman, D.S., Sydeman, W.J., 2016. Responses of Marine Organisms to Climate Change across Oceans. Front. Mar. Sci. 3, 62. https://doi.org/10.3389/fmars.2016.00062.

R Development Core Team, 2016. R: A language and environment for statistical computing. Vienna, Austria.

Rabassa, J., Heusser, C.J., Stuckenrath, R., 1986. New data on Holocene sea transgression in the Beagle Channel: Tierra del Fuego, Argentina. Quater. South Am. Antarctic Peninsula 4, 291–309.

Rabassa, J., Coronato, A., Bujalesky, G., Salemme, M., Roig, C., Meglioli, A., Heusser, C., Gordillo, S., Roig, F., Borromei, A., Quattrocchio, M., 2000. Quaternary of Tierra del Fuego, southernmost South America: an updated review. Quat. Int. 68-71, 217–240. https://doi.org/10.1016/S1040-6182(00)00046-X.

Rabassa, J., Coronato, A., Gordillo, S., Candel, M.S., Martínez, M.A., 2009. Paleoambientes litorales durante el inicio de la transgresión marina holocena en Bahía Lapataia, Canal Beagle, Parque Nacional Tierra del Fuego. Rev. Asoc. Geol. Argent. 65 (4), 648–659.

Reid, D., Osorio, C., 2000. The shallow-water marine mollusca of the Estero Elefantes and Laguna San Rafael, southern Chile. Bull. Nat. Hist. Mus. London, Zoology 66, 109–146.

Reimer, P.J., Bard, E., Bayliss, A., Beck, J.W., Blackwell, P.G., Ramsey, C.B., Buck, C.E., Cheng, H., Edwards, R.L., Friedrich, M., Grootes, P.M., Guilderson, T.P., Haflidason, H., Hajdas, I., Hatté, C., Heaton, T.J., Hoffman, D.L., Hogg, A.G., Hughen, K.A., Kaiser, K.F., Kromer, B., Manning, S.W., Niu, M., Reimer, R.W., Richards, D.A., Scott, E.M., Southon, J.R., Staff, R.A, Turney, C.S.M., Van Der Plicht, J., 2013. IntCal13 and Marine13 radiocarbon age calibration curves 0–50,000 years cal BP. Radiocarbon 55 (4), 1869–1887. https://doi.org/10.2458/azu_js_rc.55.16947.

Renssen, H., Goosse, H., Fichefet, T., Masson-Delmotte, V., Koç, N., 2005. Holocene climate evolution in the high-latitude Southern Hemisphere simulated by a coupled atmosphere-sea ice-ocean-vegetation model. The Holocene 15 (7), 951–964. https://doi.org/10.1191/0959683605hl869ra.

Reynolds, D.J., Hall, I.R., Scourse, J.D., Richardson, C.A., Wanamaker, A.D., Butler, P.G., 2017. Biological and climate controls on north atlantic marine carbon dynamics over the last millennium: insights from an absolutely dated shell-based record from the north icelandic shelf. Glob. Biogeochem. Cycles 31 (12), 1718–1735. https://doi.org/10.1002/2017gb005708.

Riascos, J.M., Avalos, C.M., Pacheco, A.S., Heilmayer, O., 2012. Testing stress responses of the bivalve Protothaca thaca to El Niño–La Niña thermal conditions. Mar. Biol. Res. 8 (7), 654–661. https://doi.org/10.1080/17451000.2011.653367.

Ridgway, I.D., Richardson, C.A., Austad, S.N., 2011. Maximum shell size, growth rate, and maturation age correlate with longevity in bivalve molluscs. J. Gerontol. Ser. A 66 (2), 183–190. https://doi.org/10.1093/gerona/glq172.

Rohlf, F.J., 1999. TpsRewl, vol. V. 1.18. University at Stony Brook, New York State.

Rohlf, F.J., 2005. TpsDig, Ver. 2.04. Department of Ecology and Evolution. State University of New York at Stony Brook.

Rosenberg, G., 2009. A Database of Western Atlantic Marine Mollusca: Malacolog 4.1.1. http://www.malacolog.org/.

Rubo, S., Aguirre, M.L., Richiano, S.M., Medina, R.A., Schöne, B.R., 2018. Leukoma antiqua (Bivalvia)-A high-resolution marine paleoclimate archive for southern South America? Palaeogeogr. Palaeoclimatol. Palaeoecol. 505, 398–409. https://doi.org/10.1016/j.palaeo.2018.06.024.

Saulsbury, J., Moss, D.M., Ivany, L.C., Kowalewski, M., Lindberg, D.R., Gillooly, J.F., Heim, N.A., McClain, C.R., Payne, J.L., Roopnarine, P.D., Schone, B.R., Goodwin, D., Finnegan, S., 2019. Evaluating the influences of temperature, primary production, and evolutionary history on bivalve growth rates. Paleobiology 45 (3), 405–420. https://doi.org/10.1017/pab.2019.20.

Schöne, B.R., Gillikin, D.P., 2013. Unraveling environmental histories from skeletal diaries — Advances in sclerochronology. Palaeogeogr. Palaeoclimatol. Palaeoecol. 373, 1–5. https://doi.org/10.1016/j.palaeo.2012.11.026.

Stanley, S.M., 1970. Relation of shell form to life habits of the Bivalvia (Mollusca), Vol. 125. Geological Society of America.

Stead, R.A., Clasing, E.L., Navarro, J.M., Asencio, G., 1997. Reproductive cycle and cohort formation of *Venus antiqua* (Bivalvia: Veneridae) in the intertidal zone of southern Chile. Rev. Chil. Hist. Nat. 70, 181–190.

Stuiver, M., Reimer, P.J., 1993. Extended 14C data base and revised. CALIB 3.0 14C Age calibration program. Radiocarbon 35, 215–230. https://doi.org/10.1017/S0033822200013904.

Turner, J., Marshall, G.J., 2011. Climate change in the polar regions. Cambridge University Press.

Urban, H.J., Campos, B., 1994. Population dynamics of the bivalves *Gari solida*, *Semele solida* and *Protothaca thaca* from a small bay in Chile at 36°S. Mar. Ecol. Progress Ser. 115, 93. https://doi.org/10.3354/meps115093.

Wanamaker, A.D., Hetzinger, S., Halfar, J., 2011. Reconstructing mid- to high-latitude marine climate and ocean variability using bivalves, coralline algae, and marine sediment cores from the Northern Hemisphere. Palaeogeogr. Palaeoclimatol. Palaeoecol. 302, 1–9. https://doi.org/10.1016/j.palaeo.2010.12.024.

Zelditch, M., Swiderski, H., Fink, W., 2004. Geometric Morphometrics for Biologist: a Primer. Elsevier Academic Press, London.